Dopant-Dependent Stability of Garnet Solid Electrolyte Interfaces with Lithium Metal

Yisi Zhu[1], Justin G. Connell[1,2], Sanja Tepavcevic[1], Peter Zapol[1], Regina Garcia-Mendez[3], Nathan J. Taylor[4], Jeff Sakamoto[3,4], Brian J. Ingram[4], Larry A. Curtiss[1], John W. Freeland[5], Dillon D. Fong[1], Nenad M. Markovic[1,]*

[1] Materials Science Division, Argonne National Laboratory, Argonne, IL 60439, USA
[2] Joint Center for Energy Storage Research, Argonne National Laboratory, Argonne, IL 60439, USA
[3] Department of Materials Science and Engineering, University of Michigan, Ann Arbor, MI 48109, USA
[4] Department of Mechanical Engineering, University of Michigan, Ann Arbor, MI 48109, USA
[5] Chemical Sciences and Engineering Division, Argonne National Laboratory, Lemont, Illinois 60439, United States
[6] X-ray Sciences Division, Argonne National Laboratory, Argonne, IL 60439, USA

* Email: nmmarkovic@anl.gov

Abstract

$Li_7La_3Zr_2O_{12}$ (LLZO) garnet-based materials doped with Al, Nb or Ta to stabilize the Li^+-conductive cubic phase are a particularly promising class of solid electrolytes for all-solid-state lithium metal batteries. Understanding of the intrinsic reactivity between solid electrolytes and relevant electrode materials is crucial to developing high voltage solid-state batteries with long lifetimes. Using a novel, surface science-based approach to characterize the intrinsic reactivity of the Li-solid electrolyte interface, we determine that, surprisingly, some degree of Zr reduction takes place for all three dopant types, with the extent of reduction increasing as Ta < Nb < Al. Significant reduction of Nb also takes place for Nb-doped LLZO, with electrochemical impedance spectroscopy (EIS) of Li||Nb-LLZO||Li symmetric cells further revealing significant increases in impedance with time and suggesting that the Nb reduction propagates into the bulk. Density functional theory (DFT) calculations reveal that Nb-doped material shows a strong preference for Nb dopants towards the interface

This is the author manuscript accepted for publication and has undergone full peer review but has not been through the copyediting, typesetting, pagination and proofreading process, which may lead to differences between this version and the Version of Record. Please cite this article as doi: 10.1002/aenm.201803440.

between LLZO and Li, while Ta does not exhibit a similar preference. EIS and DFT results, coupled with the observed reduction of Zr at the interface, are consistent with the formation of an "oxygen-deficient interphase" (ODI) layer whose structure determines the stability of the LLZO-Li interface.

1. Introduction

In the field of electrochemical energy storage, solid-state battery systems are emerging as a promising technology with advantages over conventional liquid electrolyte-based batteries that include higher energy density,[1] wider electrochemical stability window[2] and operable temperature range,[3] as well as improved safety.[4] Cubic $Li_7La_3Zr_2O_{12}$ (LLZO) garnet-based materials are a particularly promising class of solid electrolytes for all-solid-state lithium metal batteries, as they are predicted to have a wide electrochemical stability window,[5, 6] can be synthesized with very high density (>97%)[7, 8] and, through aliovalent doping, can achieve room temperature Li-ion conductivities as high as ~1.0 mS cm^{-1} with negligible electronic conductivity.[9] However, significant fundamental issues remain unresolved for garnet-based all-solid-state batteries, including low accessible current densities,[10] the persistence of Li dendrite formation,[11, 12] and perhaps most importantly, ambiguities as to whether the interfaces between LLZO and both Li metal[13, 14] and high voltage oxide cathodes[15, 16] are stable over extended cycling. Indeed, developing deep understanding of the intrinsic reactivity between solid electrolytes and relevant electrode materials is crucial to developing high voltage solid-state batteries with long lifetimes, as the presence of any significant (electro)chemical reactivity will ultimately lead to premature cell failure during extended cycling.

Understanding interfacial stability is an especially challenging issue common to all solid-state battery systems due to the inability of many experimental techniques to adequately interrogate the chemical properties of buried interfaces. Such studies are further complicated when one or both materials at the interface are unstable to exposure to air, water, etc., as the formation of unintentional reaction layers can mask the intrinsic chemistry of the interface and ultimately alter the electrochemical performance of the system. LLZO-based solid electrolytes in particular are well known to form Li_2CO_3 and LiOH when exposed to CO_2 and H_2O, respectively,[17] and it has been widely demonstrated that the formation of such reaction layers on the LLZO surface results in high interfacial impedance when in contact with Li metal.[18] Removing the Li_2CO_3/LiOH reaction layer, usually achieved via mechanical polishing, results in significantly lower interfacial impedance;[19] however, little is known about the chemistry or long-term stability of the interface between "pristine" LLZO and Li metal. Further complicating the issue of the stability of LLZO in contact with Li is understanding the role that various dopant species (used to stabilize the cubic garnet phase and improve Li^+ conductivity) play in guiding interfacial reactivity. Indeed, there is some evidence that the dopant type affects the long-term stability of LLZO in contact with Li metal.[20] However, the underlying (electro)chemical mechanisms for this behavior are still unknown.

A variety of methods have been used to characterize the chemical reactivity of Li metal and LLZO – for example, pressing Li foil onto the electrolyte material at room temperature[21] or dropping molten lithium onto the electrolyte surface[22, 23] and monitoring whether a color change takes place to indicate the presence or absence of chemical reactivity. Such approaches are limited, however, as the lithium surface can easily oxidize, even in an inert glove box environment, and the use of molten lithium characterizes reactivity beyond normal

battery operating temperatures. *In situ* scanning transmission electron microscopy (STEM) methods have also been used to directly visualize the interface between Al-doped LLZO and Li metal, providing insights into the physical extent of reaction that takes place.[24] We have recently demonstrated a surface science-based approach for characterizing the intrinsic reactivity of the buried Li-solid electrolyte interface in which lithium is sputtered onto the solid electrolyte material at room temperature, and changes in the interfacial chemistry are monitored using X-ray photoelectron spectroscopy (XPS).[25] This methodology was used to successfully identify the reduction of Nb dopant species in LLZO by Li metal, suggesting that dopants do indeed play a critical role in determining the reactivity of the LLZO-Li interface.

In this report, we extend our surface science-based approach to understand the origins of (electro)chemical stability in solid electrolyte materials by systematically studying both surface chemistry and dopant-dependent LLZO/Li interfacial reactivity. By preparing LLZO samples with different extents of surface oxidation via mechanical polishing and/or ultrahigh vacuum (UHV) annealing, the degree of interfacial reactivity with Li is shown to be strongly dependent on the initial surface chemistry. In general, surfaces with less CO_3^{2-} result in more extensive reduction of LLZO by Li. Through the use of LLZO samples with different dopant species (Nb, Ta and Al), we further determine that the chemistry of LLZO in contact with Li is strongly dependent on dopant type. Significant reduction of Nb is observed for Nb-doped samples, and at least some degree of Zr^{4+} reduction takes place for all three dopant types, with the extent of reduction increasing as Ta < Nb < Al. These results are surprising, as Nb chemical reactivity is typically similar to Ta, and Al-doped LLZO is widely assumed to be stable to Li metal.[26, 27] Electrochemical impedance spectroscopy (EIS) of Li-Li symmetric coin cells reveals that only Nb-doped LLZO exhibits significant increases in impedance with

time, whereas Al-doped and Ta-doped LLZO are stable, suggesting that the chemical reactions in the presence of Li observed for Nb-doped LLZO propagate into the bulk. Density functional theory (DFT) calculations reveal that the Nb-doped material shows a strong preference for Nb dopants to segregate toward the interface between LLZO and Li, while Ta does not exhibit a similar preference, indicating that the observed reactivity of Nb-doped LLZO with Li may be driven by a redistribution of Nb within the structure that leads to lower Zr content at the LLZO surface. Taken together, these results suggest that the stability of the LLZO-Li interface is driven by the reduction of Zr^{4+} and the formation of an "oxygen-deficient interphase" layer that protects LLZO from further reduction, with the extent of protection determined by the degree of interaction of the specific dopant species with the Zr sublattice. This work clearly demonstrates the power of our surface science-based approach to characterize buried interfaces in technologically-relevant materials for solid-state Li-ion batteries, and provides a foundation for understanding how to design new materials with improved stability and electrochemical performance.

2. Results

2.1 Influence of Surface Preparation on LLZO Surface Chemistry

Due to the wide array of LLZO surface chemistries reported in the literature,[28, 29] we begin by preparing LLZO surfaces with differing degrees of surface cleanliness in order to systematically use surface chemical analysis with XPS to understand the impact of LLZO surface chemistry on its reactivity with Li metal. Making use of the unique ability of our surface science-based approach to transfer samples directly from a glove box environment to UHV for surface analysis (see Experimental Methods for details), we ensure that the observed surface chemistry is directly representative of the surface chemistry that results

from each surface treatment. For clarity, we focus initially on the surface reactivity of polycrystalline, Nb-doped LLZO pellets (nominal composition $Li_{6.5}La_3Zr_{1.5}Nb_{0.5}O_{12}$); however, similar results **(Figure S1 and Table S1)** are obtained for both Ta- and Al-doped materials ($Li_{6.5}La_3Zr_{1.5}Ta_{0.5}O_{12}$ and $Li_{6.25}Al_{0.25}La_3Zr_2O_{12}$, respectively) as well. These LLZO compositions are chosen specifically because they exhibit the maximum Li-ion conductivity for each dopant type, making them the most relevant compositions for real battery applications.

In addition to the main LLZO peak at 530.7 eV observed by XPS analysis of the O 1s core level, the as-synthesized material **(Figure 1a)** reveals significant Li_2CO_3 (533.7 eV) and LiOH (532.8 eV) content on the surface, which are known to be the two major surface oxidation products on LLZO that form upon exposure to CO_2 and H_2O, respectively.[17] Note that the binding energies for both carbonate and hydroxyl species are ~2 eV higher than their literature values due to differential charging (see Experimental Section and **Figure S2** for more details). Li_2CO_3, in particular, is understood to result in a higher interfacial impedance,[18] and as a result, it is common practice to remove this interfacial reaction layer by mechanical polishing inside of a glove box before cell assembly.[30] XPS analysis of polished samples **(Figure 1b)** reveals that much, but not all, of the carbonate content is indeed removed upon polishing; however, significant LiOH content remains on the surface, which is most likely formed from residual H_2O present either in the glove box environment or in the polishing paper. In order to further clean the LLZO surface of reaction products, annealing of these samples was carried out in UHV at 80ºC **(Figure 1c)**, which led to removal of LiOH species. Further annealing to 500ºC **(Figure 1d)** resulted in complete removal of the Li_2CO_3, yielding a pristine LLZO surface. The annealed LLZO data represent, to our knowledge, the only reported XPS analysis of LLZO without any interfacial surface

reaction species. The relative LiOH, Li_2CO_3 and LLZO contributions to O 1s spectra for various surface treatments are summarized in Table S1, and the corresponding C 1s core level and survey spectra are shown in **Figure S2 and S3**. We note that when UHV-annealed samples are reintroduced to the glove box environment, the surface contaminants begin to reform after only 5 minutes of exposure, and return to a state similar to that of the polished surface within 3 hours **(Figure S4)**, indicating that residual CO_2 and H_2O in the glove box environment is sufficient to oxidize LLZO surfaces.

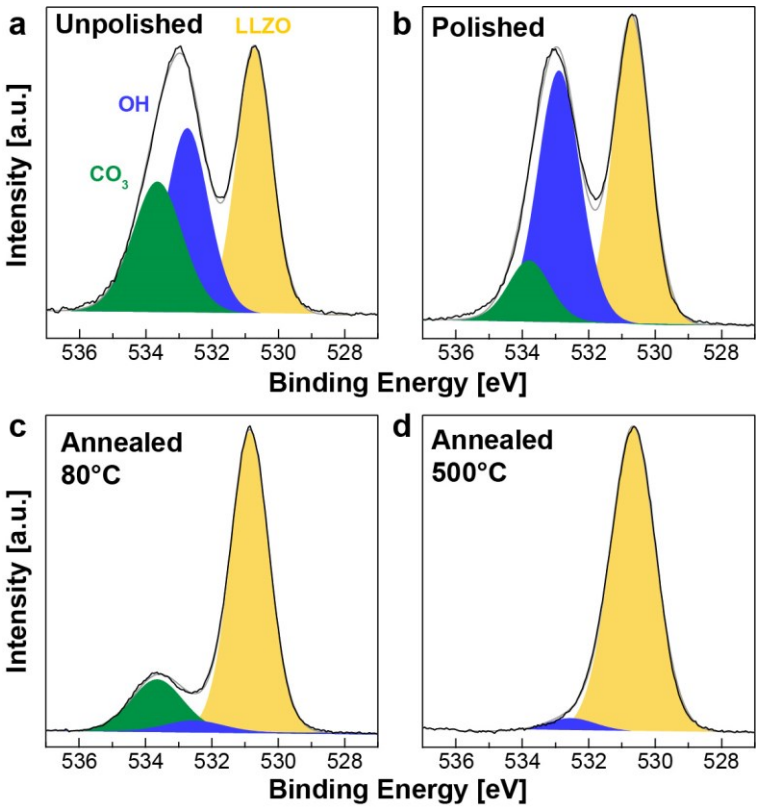

Figure 1. Representative O 1s core level XPS spectra from (a) unpolished (b) polished (c) 80°C UHV heated and (d) 500°C UHV heated Nb-doped LLZO surfaces.

2.2 Surface Chemistry and Dopant-Dependent Li Reactivity

Having demonstrated it is possible to reliably produce LLZO surfaces with varying surface chemistry, we turn our attention to understanding the impact of these surface reaction layers

on subsequent reactivity with Li metal. To ensure that the analysis of the annealed samples is representative of the intrinsic chemistry of cubic LLZO, all doped samples were monitored *in situ* with X-ray diffraction during annealing in high vacuum in a separate experiment to verify that heating to 500ºC does not result in the formation of any impurity phases (e.g., La_2ZrO_7) or decomposition products **(Figure S5)**. Three distinct surfaces – unpolished, polished and heated – were prepared for LLZO with Nb, Ta and Al doping, producing a total of 9 different LLZO surfaces. Li metal was deposited directly onto each surface for the same amount of time, after which the samples were immediately transferred under UHV conditions for XPS characterization **(Figure 2)**.[25] Results are summarized in Figure 2 for the Zr 3d core levels of all samples, as well as for the Nb 3d core level for Nb-doped samples, and a summary of the fitted peak positions for all XPS core levels in the manuscript is given in **Table S2**. No reactivity was observed for La species on any of the surfaces **(Figure S6a)**, nor for Ta in Ta-doped LLZO **(Figure S6b)**, but it was not possible to analyze Al with XPS (see Experimental Section for details).

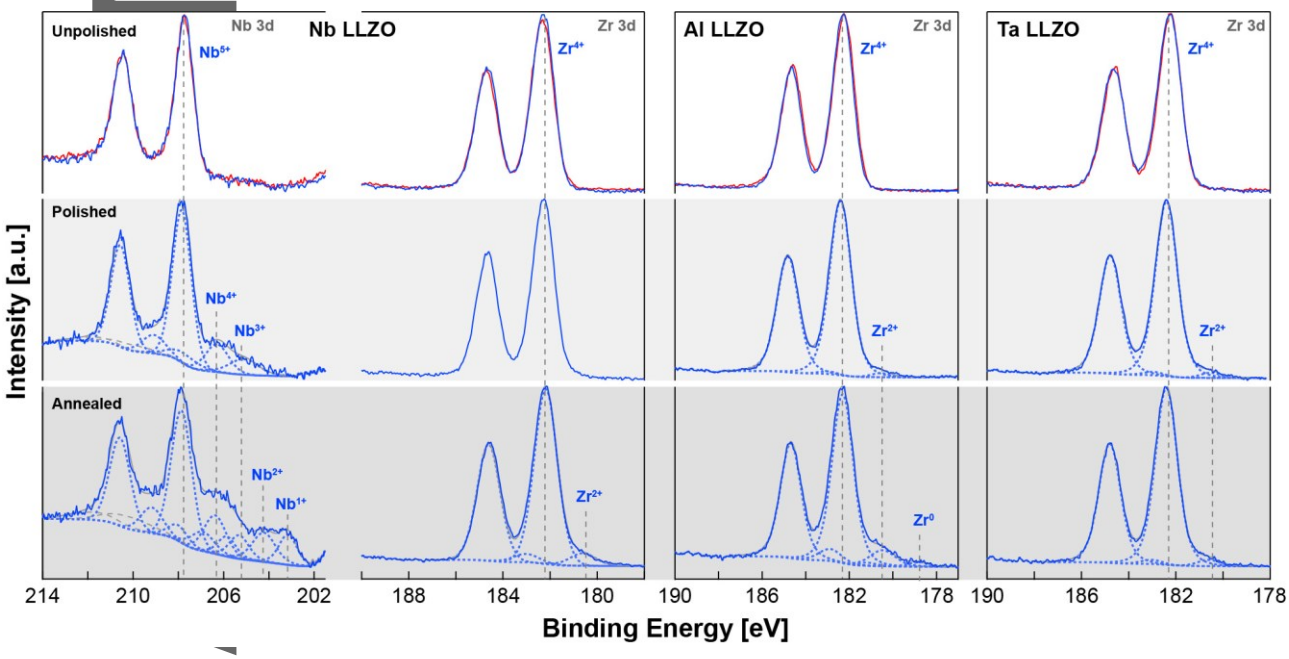

Figure 2. Nb 3d and Zr 3d core level XPS spectra from Nb-, Al- and Ta-doped LLZO with unpolished (top), polished (middle) and UHV heated (bottom) surfaces before (red) and after (blue) Li deposition. For clarity and to highlight the lack of reactivity on these surfaces, comparisons before and after Li deposition are only shown for unpolished samples.

Analysis of doped samples with unpolished surfaces **(Figure 2, top row)** indicates that, regardless of dopant type, there is essentially no interfacial reaction after Li sputtering, which is consistent with observations that Li_2CO_3-coated LLZO surfaces are not wet by Li metal and exhibit high impedance.[19] However, Li deposition onto polished, Nb-doped samples **(Figure 2, middle row)** leads to a clear reduction of Nb^{5+} to Nb^{4+} and Nb^{3+}, as evidenced by the presence of new peaks at 206.4 and 205.3 eV, respectively, with no apparent reactivity of Zr^{4+} species. In contrast to Nb-doped samples, both Al- and Ta-doped LLZO exhibit evidence of Zr^{4+} reduction with a small, but measurable, peak emerging at 180.6 eV that is consistent with the binding energy of Zr^{2+}.[31] This result is particularly surprising, as both Al- and Ta-doped LLZO are generally assumed to be stable in contact with Li metal. Zr reduction could be derived from Li^+ insertion as defined by the electro-neutrality equation (i.e., a decrease in oxygen vacancy concentration); however, it is more likely that the highly oxophilic Li metal drives the reduction of the LLZO surface, forming an oxygen-deficient interphase (ODI) layer that is charge compensated by Zr^{4+} reduction.

Li deposition onto UHV-annealed, oxidation product-free LLZO surfaces **(Figure 2, bottom row)** reveals a greater overall degree of Nb reduction, as well as the presence of additional Nb^{2+} and Nb^{1+} reduction species. Zr reduction is also observed for all three dopant types, with the Al-doped material exhibiting the greatest extent of Zr reduction as well as the presence of an additional Zr peak at 179.0 eV. This species is consistent with the peak position of Zr^0 [32] and is not present for other doped LLZO samples. Interestingly, there are several reports in the literature demonstrating that the addition of a metal interlayer (e.g., Al,

Au, Ge) to the interface between LLZO and Li metal results in a lowered interfacial impedance,[33, 34] and it is possible that the spontaneous formation of reduced Zr species at the LLZO-Li interface is what drives the observed electrochemical stability of Al-doped LLZO despite its apparent chemical reactivity. Given the low mobility of Zr[35] and the relatively small fraction of Zr^0 relative to $Zr^{4+}$and Zr^{2+}, it is unlikely that a fully metallic Zr layer is formed at the interface; however, this indicates that Al-doped LLZO forms the most extensive ODI layer out of all three dopant types. Although it was not possible to analyze the Al valence state with XPS, soft X-ray absorption measurements in total fluorescence yield mode showed no significant changes to the Al K edge after reaction with Li **(Figure S6c)**, suggesting that the Al species are stable in the bulk of LLZO and indicating that the reaction is surface-limited. We note that the observed surface treatment-dependent reactivity (i.e., unpolished < polished << UHV annealed) also corresponds with increases in the apparent Li film thickness (i.e., darker gray color), consistent with the observation that Li_2CO_3-coated surfaces are not wet by Li metal.[19]

2.3 Impact of Reactivity on Interfacial Impedance

The relative fractions of reduced species for each dopant and surface treatment are summarized in **Table 1**. Using these data, it was possible to calculate the total amount of charge transferred per formula unit of LLZO, giving a more quantitative comparison of the extent of reduction between samples. Most interestingly, UHV-annealed, Nb- and Al-doped LLZO exhibit comparable amounts of charge transfer after reaction with Li metal, with ca. 0.58 and 0.60 mol e^- transferred, respectively. This stands in strong contrast to Ta-doped LLZO, with only 0.08 mol e^- transferred at the interface, indicating that the overall trend in the extent of reduction is Al $\gtrsim$ Nb > Ta.

In order to correlate the observed interfacial reactivity with electrochemical response, electrochemical impedance spectroscopy (EIS) and galvanostatic cycling measurements of symmetric Li||LLZO||Li cells was carried out **(Figure 3 and S7)**. EIS spectra exhibit two semicircles and a low-frequency tail/semicircle, and these spectra were fit using a L-R_1-(R_2Q)-W equivalent electrical circuit model, which takes into account chemical diffusion at the interface (see Experimental Section for details). The high frequency region fits are provided in the insets of Figure 3, and the full fitting is shown in **Figure S8**. This model indicates an incomplete, first semicircle with a peak at ~300 kHz that corresponds to grain boundary conduction in the LLZO pellets. This semicircle is present in all LLZO measurements and is consistent with values reported elsewhere in the literature.[16] To verify this assignment, a separate EIS measurement was carried out from 7 MHz to 250 mHz using symmetric Au||LLZO||Au cells **(Figure S9)**, which further revealed the bulk impedance contribution and yielded grain boundary impedance response similar to that observed in Li-Li symmetric cells. Resistance and capacitance values for all fittings of EIS spectra are summarized in **Table S3** and are in good agreement with those reported elsewhere in the literature.[20, 36]

Table 1. Percentage of elemental reduction in LLZO after Li metal deposition, calculated from XPS relative peak intensities in Figure 2, and total charge transfer per mole LLZO based on the total change in oxidation state for each surface condition. Dashes (–) indicate no change.

Samples Unpolished Polished Annealed	La	Zr	Dopant	Charge Transfer per 1 mol LLZO [mol e^-]
$Li_{6.25}Al_{0.25}La_3Zr_2O_{12}$	-	-	-	0.00
	-	2.5% Zr^{2+}	Unknown	0.10
	-	9.3% Zr^{2+} 2.8% Zr^0	Unknown	0.60
$Li_{6.5}La_3Zr_{1.5}Nb_{0.5}O_{12}$	-	-	-	0.00
	-	-	16.0% Nb^{4+} 12.0% Nb^{3+}	0.20
	-	7.5% Zr^{2+}	15.9% Nb^{4+}	0.58

			9.0% Nb^{3+} 13.2% Nb^{2+} 10.8% Nb^{1+}	
$Li_{6.5}La_3Zr_{1.5}Ta_{0.5}O_{12}$	-	-	-	0.00
	-	2.5% Zr^{2+}	-	0.08
	-	2.4% Zr^{2+}	-	0.07

Symmetric Li||LLZO||Li cells exhibit an additional impedance contribution that is not present for the Au||LLZO||Au cells, which has a peak at ~1 kHz. This contribution was modeled by a ($R_{electrode}Q_{electrode}$) equivalent circuit element, yielding an equivalent capacitance value of ~10^{-6} F that is consistent with charge-transfer processes (typically 10^{-7}–10^{-5} F)[36] and is assigned to the contribution of charge transfer resistance from Li/LLZO interfacial reactivity. $R_{electrode}$ values for Al- and Ta-doped LLZO are comparable (~100 and ~50 Ω cm^2, respectively), whereas $R_{electrode}$ of

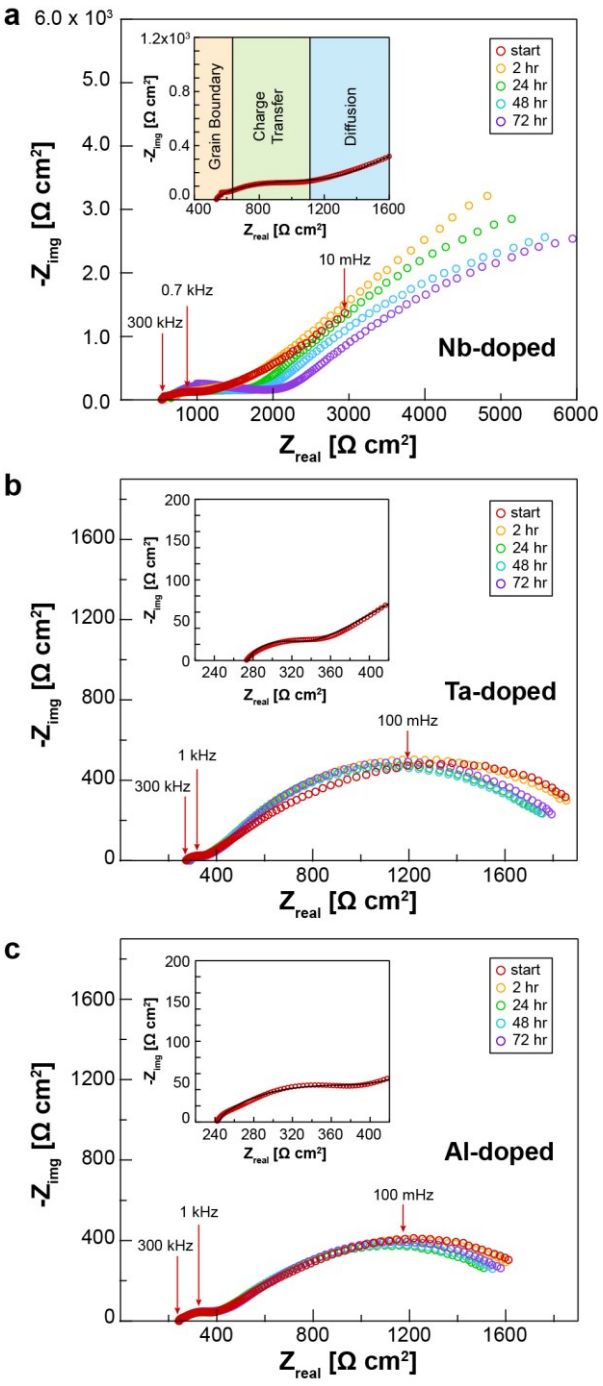

Figure 3. EIS spectra for Li-Li symmetric cells with (a) Nb (b) Ta and (c) Al-doped LLZO demonstrating the change in impedance over 72 hours due to reaction with Li metal. Insets show high frequency region equivalent circuit fitting (black line) for the initial EIS spectrum of each doped LLZO sample.

Nb-doped LLZO is ~800 Ω cm^2. These resistance values are quite low,[8] and are the result of the highly conformal Li-LLZO interface that is generated from vacuum deposition of Li

metal. Furthermore, despite the highest degree of interfacial Zr reactivity, Al-doped LLZO exhibits very low interfacial impedance (i.e., Nb >> Al > Ta), which indicates significant interfacial reactivity is not, in and of itself, a detrimental phenomenon, and may in fact lead to spontaneous stabilization of the interface. Differences in EIS response correlate directly with differences in galvanostatic cycling behavior (Figure S7), highlighting the power of our surface science-based approach to correlate chemical reactivity with electrochemical response, even without the need for charge/discharge measurements. A third semicircle is also observed in the low-frequency region of the EIS spectra, which exhibits a peak at ~0.1 Hz for Al- and Ta-doped LLZO but is not fully resolved for Nb-doped LLZO. This feature was modeled using a Warburg element in the equivalent circuit model and is attributed to the diffusion limitation of Li ions through a capacitive, partially blocking interface layer.[37] It is unclear at this time why this region is not fully resolved for Nb-doped LLZO samples; however, it is likely related to the structure of the ODI at the Nb-LLZO/Li interface that modifies the barrier to Li diffusion. For comparison, the low frequency impedance response of solid-liquid interfaces commonly observed in Li-ion batteries is strongly influenced by the structure of both the double layer and the solid electrolyte interphase.[38]

Differences in reactivity between all three dopant species are further highlighted when comparing the evolution of the interfacial impedance with time (Figure 3). Over the course of 3 days of measurements, the EIS spectra of Al- and Ta-doped samples are essentially unchanged, whereas the charge transfer resistance (R_2) of Nb-doped LLZO doubles to 1600 Ω cm^2. This suggests that the reactivity observed from XPS measurements on Al- and Ta-doped samples is surface-limited, while the reactivity on the Nb-doped material is not self-limiting and continues into the bulk. Indeed, Nb-doped LLZO samples extracted from coin cells after impedance measurements exhibit significant discoloration, whereas no

discoloration is observed for either Al- or Ta-doped material **(Figure S10)**. Additional polishing of Nb-doped samples to remove several hundreds of microns of material from the surface does not remove this discoloration, and XPS measurements of re-polished samples reveal significant reduction of Nb species in the bulk **(Figure 4a)**. It is likely that Nb reduction also results in the development of electronic conductivity, which is supported by the black color of reacted samples as well as by an observed decrease in R_1 (i.e., the portion of the bulk resistance that is resolved by our EIS measurements) from ~500 to ~300 Ω cm^{-2} after 72 hrs of reaction with Li metal. XRD measurements of reacted Nb-LLZO shows the presence of lattice expansion but no additional impurity phase formation **(Figure S11)**, which is consistent with Li insertion and indicates that the observed Nb reduction does not induce a bulk phase change. The presence of significant Nb reduction and lattice expansion in the bulk strongly suggests that additional Li inserts into the bulk as a result of the reaction with Li metal, driving the reduction of Nb as the Li content increases and essentially transforming Nb-doped LLZO from a solid electrolyte into a cathode material. In contrast to the Nb species, there is only Zr^{4+} observed in the Zr 3d core level spectrum of the re-polished sample, indicating that the reduction of Zr does not proceed further into the bulk and supporting the hypothesis that Zr^{4+} reduction is related to the formation of the ODI layer rather than Li^{+} insertion at the LLZO-Li interface. We note that no current was passed during these measurements (i.e., no Li plating/stripping), demonstrating that the observed reactivity is driven only by the intrinsic thermodynamic stability of LLZO in contact with Li metal.

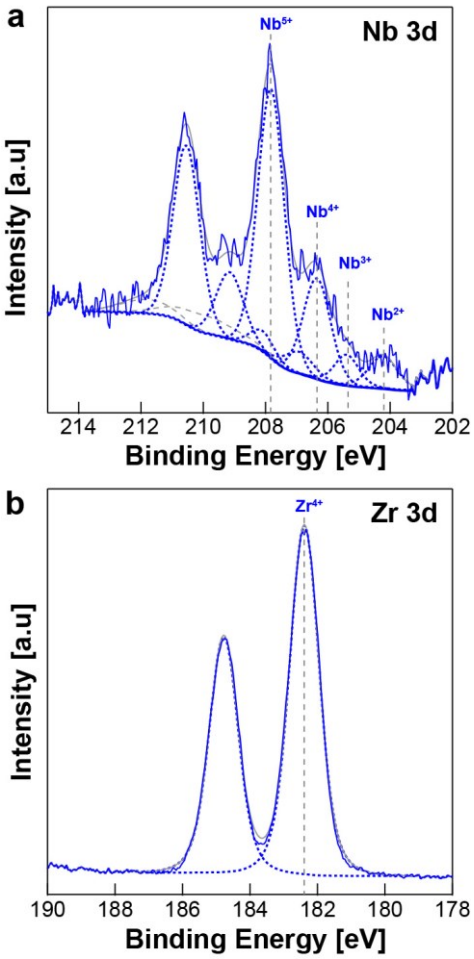

Figure 4. Nb 3d and Zr 3d core level XPS spectra from UHV heated, Nb-doped LLZO samples left in contact with Li for 3 days and subsequently polished to remove ~0.3 mm of material from the surface reveals (a) the reduction of Nb and (b) no reactivity of Zr in the bulk.

2.4 Atomistic Origins of Differences in Ta- vs. Nb-doped LLZO Reactivity

The differences in reactivity between Nb- and Ta-doped LLZO are particularly puzzling, as both Ta and Nb belong to the same group in the periodic table and have very similar chemical properties. In order to gain deeper insights into the differences in doping behavior of Ta and Nb-doped LLZO, density functional theory (DFT) calculations were performed for LLZO(100) surfaces in contact with Li metal. Previous DFT studies were focused on the stability of cation-doped LLZO ceramics and their transport properties.[5, 39-41] Our bulk and surface LLZO models were built in a similar way to those used in previous work (see

Experimental Methods and Supporting Information for additional details). Calculations for several configurations of the Li/LLZO interface were performed using four layers of Li on top of Li-terminated LLZO(100) that was undoped, Nb-doped, or Ta-doped with nearly the same doping levels as the samples discussed above. We have calculated several instances for each dopant and report averaged energy values, since energy deviations from these averages are, in most cases, below 0.1 eV per dopant atom. The interface energy does not depend considerably on the doping element, which is explained by the fact that the top layer of the surface that interacts with deposited Li metal consists of Li and O atoms, with dopant atoms well underneath the top layer. This energy is -0.51 J/m^2, -0.52 J/m^2 and -0.55 J/m^2 for average Nb-doped, Ta-doped and undoped material, respectively. Calculations of the electronic density of states (DOS) for doped and undoped structures are characterized primarily by the addition of metallic states of adsorbed Li spanning the band gap **(Figure S12)**, and small variations observed in the DOS for the Nb- vs. Ta-doped material are insufficient to explain the observed differences in the stability of Ta- and Nb-doped LLZO.

We also considered two different dopant distributions for each dopant type, with the dopants evenly distributed in the bulk or segregated towards the surface **(Figure 5a-b)**, and at least three different configurations (i.e. particular instances of dopant positions) calculated for each distribution **(Figure S13)**. Note that here we refer to the substitutional Zr sites below the outermost Zr layers of the slab as "bulk". We find that, in the case of Ta-doped LLZO, the average energy of configurations with dopant atoms distributed near the surface vs. distributed in the bulk is nearly the same, favoring the bulk by less than 0.01 eV/dopant atom both in the presence of Li on the surface and without Li metal **(Figure 5c)**. Strikingly, in case of Nb-doped LLZO there is a strong preference for Nb to be near the surface as compared to

distributed within the bulk, both with and without Li on the surface. The average energy differences for the two distributions are 0.23 and

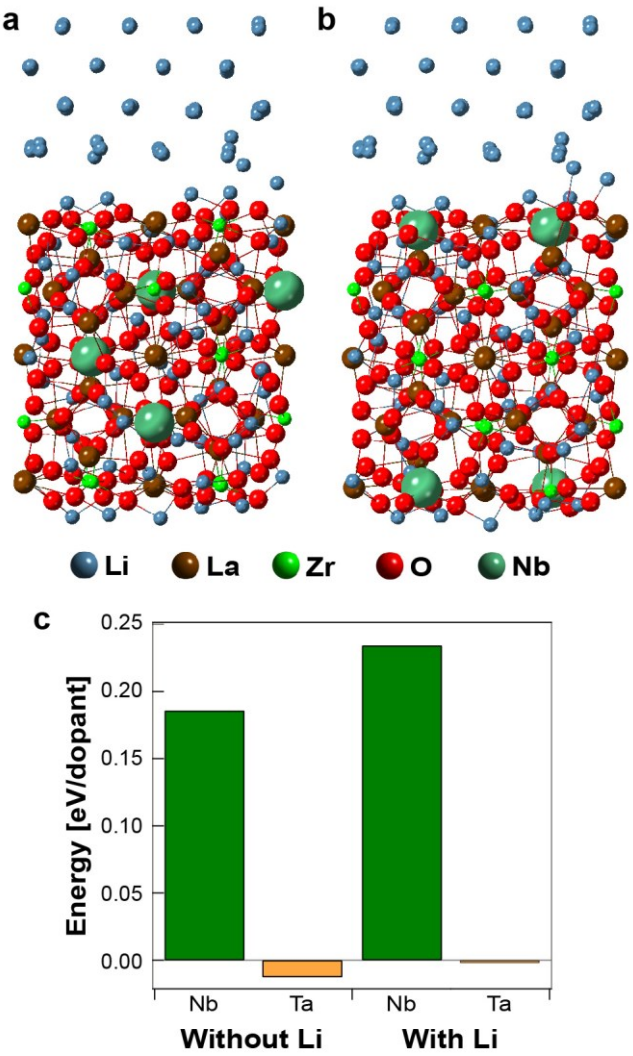

Figure 5. Examples of DFT optimized structures with Nb dopants (a) distributed in the bulk and (b) distributed towards the surface for Nb-doped LLZO in contact with Li. (c) Bar chart showing average differences in total energy near the surface and in the bulk for Nb- and Ta-doped LLZO without and with Li metal on the surface.

0.19 eV/dopant, respectively. This clearly indicates that Nb has a thermodynamic preference to substitute Zr sites near the surface of LLZO, whereas Ta has about the same preference for surface and bulk sites. The preference of Nb to occupy Zr sites near the surface is slightly stronger in the presence of deposited Li metal, which suggests that segregation of Nb to the

Li-LLZO interface may drive the high degree of reactivity of this material. This high degree of reactivity may further lead to the observed propagation of the reaction into the bulk of the material. Additional comparison of thermodynamic stability calculations with reference to Nb and Ta oxides supports the preference of Nb to be near the Li/LLZO interface (see Supporting Information for more details).

3. Discussion

Taken together, the above experimental and theoretical results suggest that the dopant-dependent stability observed for LLZO materials is driven by an interplay between the nature/distribution of dopant species present at the Li-LLZO interface and the resulting reduction of Zr^{4+} to form the oxygen-deficient interphase layer. Proposed differences in the interfacial

composition/structure are summarized schematically in **Figure 6**. In all cases, the formation of the ODI likely creates a gradient in chemical potential from Li metal to the bulk of LLZO, with the completeness and extent of formation of this layer influencing the resulting interfacial impedance. As both Nb and Ta act as substitutional dopants for Zr, the distribution of dopants within the Zr sublattice will necessarily influence the formation and electronic structure of the ODI. As the DFT results indicate a strong preference for Nb species to segregate to the surface of LLZO, it is likely that this difference in distribution drives the differences in Zr reactivity on Nb-doped LLZO relative to Ta-doped material. In the case of Ta-doped LLZO, Ta is both homogeneously distributed and stable to Li metal, leading to an overall more stable surface. The stability of Ta to reduction likely leads to a thinner ODI layer as well, which would explain the relatively low extent of Zr reduction in this material relative to the other dopant types. In contrast, the presence of enhanced Nb content at the

interface, combined with the significant reduction of Nb that takes place in contact with Li, leads to disruption and destabilization of the ODI, enabling the observed propagation of the reaction into the bulk of Nb-doped LLZO despite the more extensive Zr reduction relative to the Ta-doped material.

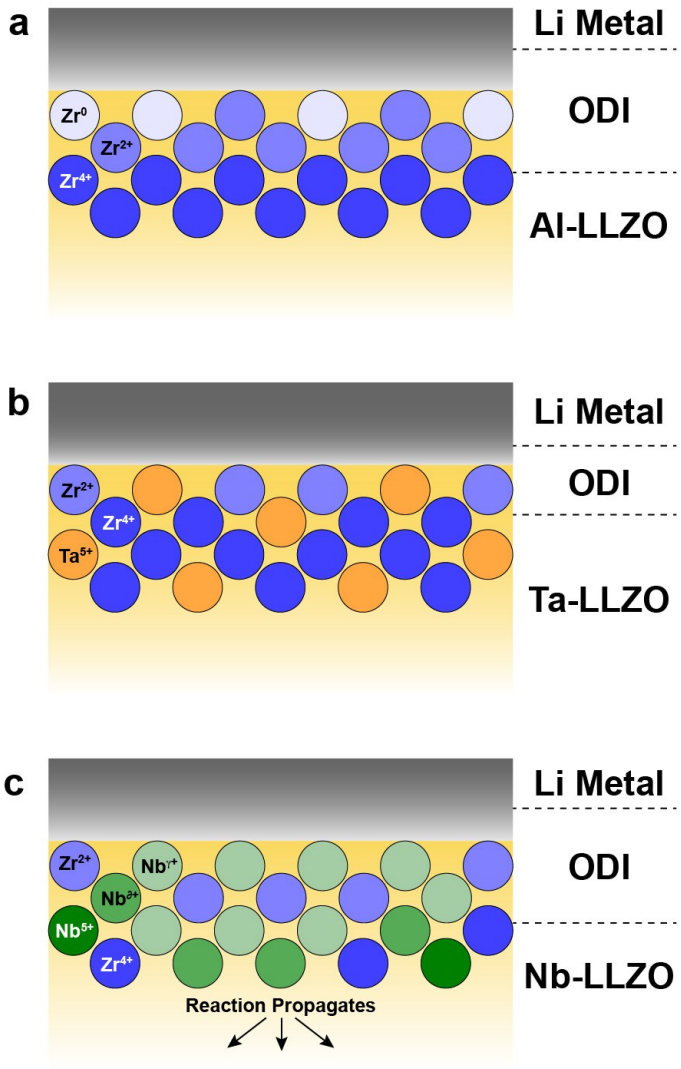

Figure 6. Schematic illustrations of the hypothesized impact of dopant type on the chemical makeup of the Zr sublattice and the resulting structure/thickness of the oxygen deficient interphase in contact with Li metal. Note that Al dopants are intentionally omitted from (a), as they do not substitute for Zr. The color gradient in the Li layer indicates oxygen segregation into the metal. $Nb^{\partial+}$ is used to denote less reduced Nb^{4+} and Nb^{3+} species, and $Nb^{\gamma+}$ is used to denote highly reduced Nb^{2+} and Nb^{1+} species.

Although XPS is unable resolve the presence or absence of Nb surface segregation due to the relatively low fraction of Nb present in LLZO (ca. 2 at%), Al-doped LLZO serves as a useful comparison as it exhibits comparable Zr reactivity to Nb-doped LLZO. As Al serves as a substitutional dopant on the Li sites in LLZO, it should not influence the distribution of Zr at the interface at all, enabling the formation of a nominally "complete" ODI layer. The larger relative fraction of reduced Zr and the presence of a small amount of Zr^0 species indicate that the ODI is likely more continuous than that formed on Nb-doped LLZO, and this layer is also thicker than that formed on Ta-doped material. The formation of a thick and/or more complete ODI prevents propagation of the reaction into the bulk, resulting in the comparably stable time-dependent impedance response to that of Ta-doped LLZO. The existence of the ODI layer is corroborated by previous *in situ* STEM imaging of the Al-doped LLZO-Li interface, which revealed the formation of a ca. 5 unit cell reaction layer.[24] Such a layer is consistent with the extent of reduction observed via XPS in this study.

4. Conclusion

By applying our unique, surface science-based approach to investigate the intrinsic stability of LLZO with different dopants and surface oxidation states in contact with lithium, it is possible to determine the underlying chemical phenomena that govern the stability of this system. Experimental and theoretical results reveal that the stability of the LLZO-Li interface is strongly related to both the initial surface chemistry and the type of dopant element present. As surface oxidation products are systematically removed, a general trend of increasing interfacial reactivity is observed. Surprisingly, reduction of Zr^{4+} is observed for all doped LLZO samples, consistent with the formation of an oxygen-deficient interphase (ODI) layer. The extent of ODI formation increases as Ta < Nb < Al. Despite the significant Zr reduction

observed on Al-doped surfaces, EIS results show that the Al-doped material possesses comparable impedance response to Ta-doped LLZO, indicating that the more extensive ODI layer formation on Al-doped LLZO serves to stabilize this material to reactivity with Li and maintains a low interfacial impedance. In contrast, Nb-doped LLZO, which exhibits slightly less Zr reduction than the Al-doped material, yields the highest impedance interface with Li. Furthermore, the impedance of the Nb-LLZO/Li interface increases with time, which is consistent with the propagation of the reaction into the bulk. DFT calculations suggest that Nb dopants have a thermodynamic preference to segregate to the LLZO surface and an even stronger preference for the Li/LLZO interface, whereas Ta dopants are nearly isoenergetic in the bulk and at the interface. This preference for surface segregation likely explains the poor stability of Nb-doped LLZO in the presence of Li, as Nb surface segregation would destabilize formation of the ODI layer. These results highlight that it will only be possible to design a new generation of highly stable materials for solid-state batteries through the development of detailed understanding of both interfacial stability and its impact on materials performance.

5. Experimental Section

Surface Preparation: Al-, Ta- and Nb-doped LLZO pellets with >97% density were synthesized as reported previously.[42,43] Samples were then prepared for surface analysis via three different treatments - unpolished, polished and UHV-annealed. Unpolished material represents the as-synthesized surface that was stored inside the glove box atmosphere (H_2O and O_2 < 0.5 ppm) for several days. Polished surfaces were prepared by sanding with 800 and 1200 grit paper, removing >1 μm of material from the LLZO surface, and were then immediately transferred into the UHV system to prevent any further oxidation. Some of these

polished surfaces were heated in the XPS analysis chamber up to 500°C with a heating rate ~ 100°C/hour in order to remove residual oxidation species that remained on the LLZO surface after polishing.

Experiment Overview: We employed a surface science-based approach identical to that described previously to study the reactivity of Nb-doped STO and LLZO materials.[25] Summarized briefly, LLZO samples with various dopants and surface treatments were first characterized with XPS in the surface analysis module of our interconnected, UHV system, then transferred under UHV conditions (10^{-10} Torr base pressure, $\leq 10^{-9}$ Torr during transfer) to the sputter deposition module for lithium deposition. Li was deposited for 30 minutes for all samples. Immediately after Li deposition, samples were transferred back to the XPS chamber to measure any reactivity that takes place as a result of contact with Li metal.

X-ray Photoelectron Spectroscopy: XPS measurements were performed using a Specs PHOIBOS 150 hemispherical energy analyzer with a monochromated Al Kα X-ray source. Charge neutralization was carried out for insulating LLZO samples using a low-energy flood gun (5 eV electron energy), with the neutralization conditions optimized on the basis of the degree of charging present for a given sample. Survey spectra were measured using a pass energy of 40 eV at a resolution of 0.2 eV/step and a total integration time of 0.1 s/point. Core-level spectra were measured using a pass energy of 20 eV at a resolution of 0.05 eV/step and a total integration time of 0.5 s/ point. It was not possible to analyze the Al 2s or 2p core level regions due to spectral overlap with the Cu 3s and 3p core levels, respectively, which are present due to Cu impurities in the Li sputter target (ca. 2-4 at%).[25] Deconvolution was performed using CasaXPS software with a Shirley-type background and

70−30 Gaussian−Lorentzian peak shapes. The use of adventitious carbon in the C 1s at 284.8 eV resulted in an unreliable charge referencing strategy, as carbon species were mostly reduced/removed by Li deposition. Furthermore, differential charging between the surface adventitious carbon/Li_2CO_3/LiOH layer and underlying LLZO resulted in LLZO peak positions at lower BE than expected. As a result, Cu metal (present as an impurity in the Li) was used as a charge reference, with the position of unreacted Zr^{4+} in the Zr 3d spectrum then used as a charge reference for samples without Li deposited to ensure self-consistent charge referencing for LLZO. This charge referencing scheme resulted in reproducible peak positions for unreacted Nb^{5+}, Ta^{5+} and La^{3+} species as well, confirming the validity of this charge referencing approach.

Coin Cell Assembly and Electrochemical Impedance Spectroscopy: Thicker lithium films were deposited on both sides of UHV-annealed LLZO pellets for EIS measurements (2 hrs total with reduced sample-target distance). After sputtering Li onto one side of the pellet, the sample was removed from UHV and a clean Li foil was placed onto the Li film to prevent direct contact between the Li film and the stainless steel sample holder after flipping over to coat the other side. After depositing on Li the back side, samples were transferred back into glove box and another clean Li foil was placed on the freshly deposited Li film. The Li-LLZO-Li symmetric cell was then assembled into a coin cell inside the same glove box. Impedance measurements of assembled symmetric coin cell were performed using a potentiostat with a Frequency Response Analyzer (FRA) module (Metrohm Autolab, Herisau, Switzerland) capable of monitoring frequencies between 1 MHz and 10 mHz. All measurements were taken at room temperature outside of the glove box, and time-dependent

measurements were taken over the full frequency range at various time intervals over the course of three days.

EIS data were fitted with an equivalent circuit model consisting of a series connection of the following elements: an inductor (L), a resistor (R_1), a parallel element consisting of a resistor (R_2) and constant phase element (Q), and a generalized finite Warburg element (W). The resulting circuit is summarized: L-R_1-(R_2Q)-W. The high frequency arc (and offset resistance) represent the overall bulk lithium transport, and are modeled by the L-R_1 series contribution to the equivalent circuit model. The parallel (R_2Q) element models the contribution of charge transfer resistance to the EIS spectrum. Although the specific mechanism contributing to the low frequency arc represented by the Warburg diffusion element is not fully understood, it is consistent with capacitive double layer formation in the LLZO pellets [37]. Qualitative comparisons between spectra provide useful insight into dopant-dependent interfacial impedance.

Density Functional Theory: DFT calculations were performed using the Vienna Ab initio Simulation Package (VASP),[44] periodic boundary conditions, and a plane wave basis set with a 500 eV kinetic energy cutoff. The core electrons were described by the projector-augmented-wave (PAW) potentials[45, 46] and the generalized gradient approximation (GGA) was used with the Perdew, Burke, Ernzerhof (PBE) exchange–correlation functional.[47] The structure optimizations for surface calculations were performed for all atomic positions within the slab model with fixed in-plane surface cell parameters to the optimized bulk value (-13.026 Å) and at least 15Å of vacuum space between periodic images. Forces were converged to at least 0.2 eV/A. Special k-points selected using the Monkhorst–Pack[48] scheme were generated with 2x2x2 set for cubic conventional LLZO unit cell. The

stoichiometry of $Li_7La_3Zr_2O_{12}$ with a conventional bulk unit cell of 192 atoms results in a partial occupation of 24d tetrahedral sites and 96h octahedral sites, with observed experimental occupancies of 0.564 and 0.442, respectively.[49] The structure for first principles calculations utilizes occupancies of 0.542 and 0.448, respectively, with the Li distribution obtained following previous recipes that minimize the occupancy of energetically unfavorable nearest-neighbor sites.[39, 49] Previous studies on the dependence of the surface energy of various LLZO orientations and terminations identified Li-terminated (100) and (110) surfaces as the most stable,[5] and we have used Li-terminated LLZO(100) in our study. The interface energy is defined as the energy difference between the slab with adsorbed Li and the sum of separated surface slab without Li and a slab of Li.

Acknowledgements

Research at Argonne National Laboratory was funded by the U.S. Department of Energy, and support from Tien Duong of the Office of Energy Efficiency and Renewable Energy Vehicle Technologies Program is gratefully acknowledged. We also acknowledge support from the Office of Science, Office of Basic Energy Sciences and Materials Sciences and Engineering Division. Li sputtering, XPS and EIS measurements were performed at the Electrochemical Discovery Laboratory, a Joint Center for Energy Storage Research facility at Argonne National Laboratory. Work at the Advanced Photon Source, Argonne was supported by the U.S. Department of Energy, Office of Science under Grant No. DEAC02-06CH11357.

References

[1] Y. Kato, S. Hori, T. Saito, K. Suzuki, M. Hirayama, A. Mitsui, M. Yonemura, H. Iba, R. Kanno, *Nat. Energy* **2016**, *1*, 16030.

[2] Z. Zhang, Y. Shao, B. Lotsch, Y.-S. Hu, H. Li, J. Janek, L. F. Nazar, C.-W. Nan, J. Maier, M. Armand, L. Chen, *Energy Environ. Sci.* **2018**, *11*, 1945.

[3] A. Manthiram, X. Yu, S. Wang, *Nat. Rev. Mater.* **2017**, *2*, 16103.

[4] J. Janek, W. G. Zeier, *Nat. Energy* **2016**, *1*, 16141.

[5] T. Thompson, S. Yu, L. Williams, R. D. Schmidt, R. Garcia-Mendez, J. Wolfenstine, J. L. Allen, E. Kioupakis, D. J. Siegel, J. Sakamoto, *ACS Energy Lett.* **2017**, *2*, 462.

[6] Y. Zhu, X. He, Y. Mo, *J. Mater. Chem. A* **2016**, *4*, 3253.

[7] T. Thompson, A. Sharafi, M. D. Johannes, A. Huq, J. L. Allen, J. Wolfenstine, J. Sakamoto, *Adv. Energy Mater.* **2015**, *5*, 1500096.

[8] X. Han, Y. Gong, K. Fu, X. He, G. T. Hitz, J. Dai, A. Pearse, B. Liu, H. Wang, G. Rubloff, Y. Mo, V. Thangadurai, E. D. Wachsman, L. Hu, *Nat. Mater.* **2017**, *16*, 572.

[9] J. Van Den Broek, S. Afyon, J. L. Rupp, *Adv. Energy Mater.* **2016**, *6*, 1600736.

[10] A. Sharafi, H. M. Meyer, J. Nanda, J. Wolfenstine, J. Sakamoto, *J. Power Sources* **2016**, *302*, 135.

[11] F. Shen, M. B. Dixit, X. Xiao, K. B. Hatzell, *ACS Energy Lett.* **2018**, *3*, 1056.

[12] B. Wu, S. Wang, J. Lochala, D. Desrochers, B. Liu, W. Zhang, J. Yang, J. Xiao, *Energy Environ. Sci.* **2018**, *11*, 1803.

[13] C. Yang, K. Fu, Y. Zhang, E. Hitz, L. Hu, *Adv. Mater.* **2017**, *29*, 1701169.

[14] F. Han, Y. Zhu, X. He, Y. Mo, C. Wang, *Adv. Energy Mater.* **2016**, *6*, 1501590.

[15] K. Park, B.-C. Yu, J.-W. Jung, Y. Li, W. Zhou, H. Gao, S. Son, J. B. Goodenough, *Chem. Mater.* **2016**, *28*, 8051.

[16] G. Vardar, W. J. Bowman, Q. Lu, J. Wang, R. J. Chater, A. Aguadero, R. Seibert, J. Terry, A. Hunt, I. Waluyo, D. D. Fong, A. Jarry, E. J. Crumlin, S. L. Hellstrom, Y.-M. Chiang, B. Yildiz, *Chem. Mater.* **2018**, *30*, 6259.

[17] A. Sharafi, S. Yu, M. Naguib, M. Lee, C. Ma, H. M. Meyer, J. Nanda, M. Chi, D. J. Siegel, J. Sakamoto, *J. Mater. Chem. A* **2017**, *5*, 13475.

[18] L. Cheng, E. J. Crumlin, W. Chen, R. Qiao, H. Hou, S. F. Lux, V. Zorba, R. Russo, R. Kostecki, Z. Liu, *Phys. Chem. Chem. Phys.* **2014**, *16*, 18294.

[19] A. Sharafi, E. Kazyak, A. L. Davis, S. Yu, T. Thompson, D. J. Siegel, N. P. Dasgupta, J. Sakamoto, *Chem. Mater.* **2017**, *29*, 7961.

[20] Y. Kim, A. Yoo, R. Schmidt, A. Sharafi, H. Lee, J. Wolfenstine, J. Sakamoto, *Front. Energy Res.* **2016**, *4*, 20.

[21] H. El Shinawi, J. Janek, *J. Power Sources* **2013**, *225*, 13.

[22] J. Wolfenstine, J. L. Allen, J. Read, J. Sakamoto, *J. Mater. Sci.* **2013**, *48*, 5846.

[23] C. Wang, Y. Gong, B. Liu, K. Fu, Y. Yao, E. Hitz, Y. Li, J. Dai, S. Xu, W. Luo, E. D. Wachsman, L. Hu, *Nano Lett.* **2017**, *17*, 565.

[24] C. Ma, Y. Cheng, K. Yin, J. Luo, A. Sharafi, J. Sakamoto, J. Li, K. L. More, N. J. Dudney, M. Chi, *Nano Lett.* **2016**, *16*, 7030.

[25] J. G. Connell, Y. Zhu, P. Zapol, S. Tepavcevic, A. Sharafi, J. Sakamoto, L. A. Curtiss, D. D. Fong, J. W. Freeland, N. M. Markovic, *ACS Appl. Mater. Interfaces* **2018**, *10*, 17471.

[26] L. Cheng, J. S. Park, H. Hou, V. Zorba, G. Chen, T. Richardson, J. Cabana, R. Russo, M. Doeff, *J. Mater. Chem. A* **2014**, *2*, 172.

[27] M. Kotobuki, K. Kanamura, Y. Sato, T. Yoshida, *J. Power Sources* **2011**, *196*, 7750.

[28] L. Cheng, C. H. Wu, A. Jarry, W. Chen, Y. Ye, J. Zhu, R. Kostecki, K. Persson, J. Guo, M. Salmeron, G. Chen, M. Doeff, *ACS Appl. Mater. Interfaces* **2015**, *7*, 17649.

[29] R. H. Brugge, A. K. O. Hekselman, A. Cavallaro, F. M. Pesci, R. J. Chater, J. A. Kilner, A. Aguadero, *Chem. Mater.* **2018**, *30*, 3704.

[30] M. Wang, J. Sakamoto, *J. Power Sources* **2018**, *377*, 7.

[31] I. Bespalov, M. Datler, S. Buhr, W. Drachsel, G. Rupprechter, Y. Suchorski, *Ultramicroscopy* **2015**, *159*, 147.

[32] C. Sleigh, A. P. Pijpers, A. Jaspers, B. Coussens, R. J. Meier, *J. Electron Spectrosc. Relat. Phenom.* **1996**, *77*, 41.

[33] Y. Lu, X. Huang, Y. Ruan, Q. Wang, R. Kun, J. Yang, Z. Wen, *J. Mater. Chem. A* **2018**, *6*, 18853.

[34] W. Luo, Y. Gong, Y. Zhu, Y. Li, Y. Yao, Y. Zhang, K. Fu, G. Pastel, C. F. Lin, Y. Mo, *Adv. Mater.* **2017**, *29*, 1606042.

[35] J. Davies, B. Domeij, J. Pringle, F. Brown, *J. Electrochem. Soc.* **1965**, *112*, 675.

[36] J. T. S. Irvine, D. C. Sinclair, A. R. West, *Adv. Mater.* **1990**, *2*, 132.

[37] W. E. Tenhaeff, E. Rangasamy, Y. Wang, A. P. Sokolov, J. Wolfenstine, J. Sakamoto, N. J. Dudney, *ChemElectroChem* **2014**, *1*, 375.

[38] M. Itagaki, S. Yotsuda, N. Kobari, K. Watanabe, S. Kinoshita, M. Ue, *Electrochim. Acta* **2006**, *51*, 1629.

[39] S. Yu, R. D. Schmidt, R. Garcia-Mendez, E. Herbert, N. J. Dudney, J. B. Wolfenstine, J. Sakamoto, D. J. Siegel, *Chem. Mater.* **2015**, *28*, 197.

[40] L. J. Miara, S. P. Ong, Y. Mo, W. D. Richards, Y. Park, J.-M. Lee, H. S. Lee, G. Ceder, *Chem. Mater.* **2013**, *25*, 3048.

[41] L. J. Miara, W. D. Richards, Y. E. Wang, G. Ceder, *Chem. Mater.* **2015**, *27*, 4040.

[42] J. L. Allen, J. Wolfenstine, E. Rangasamy, J. Sakamoto, *J. Power Sources* **2012**, *206*, 315.

[43] E. Rangasamy, J. Wolfenstine, J. Sakamoto, *Solid State Ionics* **2015**, *206*, 28.

[44] G. Kresse, J. Hafner, *Phys. Rev. B* **1993**, *47*, 558.

[45] P. E. Blochl, *Phys. Rev. B* **1994**, *50*, 17953.

[46] G. Kresse, D. Joubert, *Phys. Rev. B* **1999**, *59*, 1758.

[47] J. P. Perdew, K. Burke, M. Ernzerhof, *Phys. Rev. Lett.* **1996**, *77*, 3865.

[48] H. J. Monkhorst, J. D. Pack, *Phys. Rev. B* **1976**, *13*, 5188.

[49] H. Xie, J. A. Alonso, Y. Li, M. T. Fernández-Díaz, J. B. Goodenough, *Chem. Mater.* **2011**, *23*, 3587.

TOC Graphic and Summary

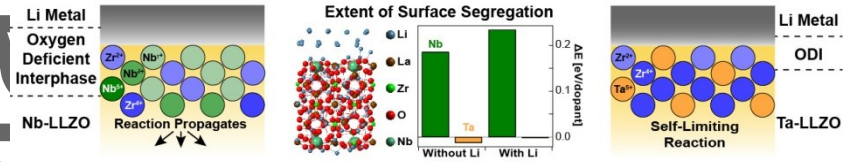

Understanding reactivity at buried interfaces is crucial to developing next-generation solid-state batteries. A novel, surface science-based approach reveals that contact with Li metal yields Zr reduction in Nb-, Ta- and Al-doped $Li_7La_3Zr_2O_{12}$, with reduction increasing as Ta < Nb < Al. This Zr reduction indicates the formation of an "oxygen-deficient interphase," whose composition determines the stability of the Li-LLZO interface.